

DESIGN, ANALYSIS, AND OPTIMIZATION OF A NEW TWO-DOF ARTICULATED MULTI-LINK ROBOTIC TAIL

Yujiong Liu, Pinhas Ben-Tzvi*
 Robotics and Mechatronics Laboratory
 Virginia Tech
 Blacksburg, VA, USA

ABSTRACT

Based on observations from nature, tails are believed to help animals achieve highly agile motions. Traditional single-link robotic tails serve as a good simplification for both modeling and implementation purposes. However, this approach cannot explain the complicated tail behaviors exhibited in nature where multi-link structures are more commonly observed. Unlike its single-link counterpart, articulated multi-link tails essentially belong to the serial manipulator family which possesses special transmission design challenges. To address this challenge, a cable driven hyper-redundant design becomes the most used approach. Limited by cable strength and elastic components, this approach suffers from low frequency responses, inadequate generated inertial loading, and fragile hardware, which are all critical drawbacks for robotic tails design. To solve these structure related shortcomings, a multi-link robotic tail made up of rigid links is proposed in this paper. The new structure takes advantage of the traditional hybrid mechanism architecture, but utilizes rigid mechanisms to couple the motions between i^{th} link and $i + 1^{\text{th}}$ link rather than using cable actuation. By doing so, the overall tail becomes a rigid mechanism which achieves quasi-uniform spatial bending for each segment and allows performing highly dynamic motions. The mechanism and detailed design for this new tail are synthesized. The kinematic model was developed and an optimization process was conducted to minimize the bending non-uniformity for the rigid tail.

1 INTRODUCTION

Tails are widely used in nature to help animals accomplish agile motions. For instance, a cheetah [1] is observed to use a tail to maneuver during hunting. Attracted by the fascinating animal tail behaviors, both scientists and engineers began to investigate the non-biological tail functionalities in recent years

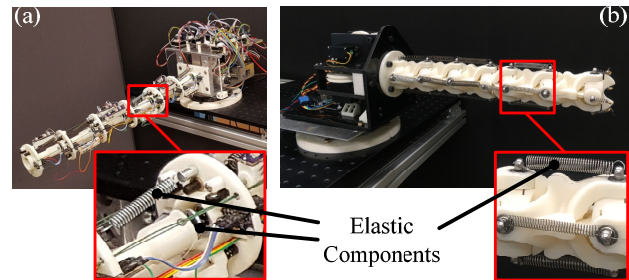


Figure 1. Two examples of multi-link flexible tails: (a) the USRT [10], (b) the RML Tail [11]. They all use elastic component (springs) to constrain the redundant DOFs.

and seriously consider its engineering potential [2].

As the first step, most researchers abstract the tail animal as a single-link pendulum. This approach brings obvious benefits: by modeling and implementing tail as one rigid body, the analysis and prototyping can be simplified significantly. The research in [1, 3-7] revealed that the tail has important effects on animal locomotion, especially for highly agile transient behaviors, such as accelerating, maneuvering, and stabilization. However, the single-link model has a fundamental drawback in that the animals in nature evolved multi-link structure tails. This makes the single-link approach unable to explain the complicated tail behaviors exhibited in nature.

Therefore, multi-link tails are proposed for both modeling and implementation purposes. Theoretical research [8] shows that the multi-link structure has the benefit of generating a higher inertial loading and volumetric center of mass workspace. Based on this finding, several multi-link robotic tails [9-11, 18, 19] were built to evaluate their practical performances. Hardware in the loop (HIL) experiments and simulations [12] were also conducted to investigate the stabilization control and maneuver control of the tail on legged

*Corresponding author – bentzvi@vt.edu

Table 1. Robotic tail structure review

Robots	Type	DOF	Planar/Spatial	Rigidity	Inter-Link Connection	Transmission
[3-4],[6-7]	Single-link	1	Planar	Rigid	-	Gear
[1]	Single-link	2	Spatial	Rigid	-	Gear
[9]	Multi-link	3	Spatial	Rigid	Revolute Joint	Cable and Gear
[10-11]	Multi-link	4	Spatial	Flexible	Universal Joint	Cable

robot locomotion. However, due to the limitations of cable strength and elastic effects of the spring components, the tails were found hard to respond high frequency input, which is critical for the success of highly dynamic robotic tails. The motivation for this work is to search for the new tail structures that can address these.

For multi-link tail designs, the current approaches roughly fit into two paradigms based on the source inspiration. The first paradigm evolved from the existed continuum manipulator [13] by discretizing the continuum backbone into multiple links and drives each link by cables or rods. The tails belonging to this category (such as the tails in [10] and [11]) usually have a hyper redundant structure and thus require additional constraints. Similar to continuum arms, elastic components are used to provide these constraints, as shown in Fig. 1. The other paradigm (such as the tail in [9]) comes more directly from an engineering framework. By analyzing the required mobility for maneuvering and stabilizing the mobile platform, it is found that two degree of freedom (DOF) planar bending plus one overall rolling DOF might be adequate for these tasks.

Both paradigms utilized cables to drive the system which suffer from cable strength limitations and cable elasticity. Other common issues for cable driven system include unidirectional driving (requires more actuators and increases control complexity), unpredictable cable friction, and relatively short lifetimes. These shortcomings worsen the low frequency response problem introduced by the elastic components.

Therefore, this paper is motivated by looking for new multi-link tail structures that are able to generate high momentums while having a high stiffness. By analyzing the relationship between the mechanical structure and the performance, a novel rigid tail based on the rigid coupling hybrid mechanism (RCHM) concept is proposed and analyzed. Corresponding kinematic and dynamic performances are evaluated for future prototyping.

The rest of this paper is organized as follows. Section 2 analyzes the design requirements and introduces the rigid coupling hybrid mechanism concept. Section 3 substantiates the robot by synthesizing the required mechanism and detailing the mechanical design. Section 4 develops the kinematic model for the proposed mechanism and Section 5 evaluates the theoretical performance based on the dynamical model.

2 FROM FLEXIBLE TAIL TO RIGID TAIL

As presented in introduction, this paper is motivated by looking for rigid multi-link tails that respond high frequency input and enable to generate high momentum. This section

analyzes the design requirements in further detail and addresses the challenge by introducing the rigid coupling hybrid mechanism.

Table 1 summarizes the mechanical structure of several typical tails (limited by the reference space, this table is not able to include all existed research. The reader is referred to [2] for more comprehensive information in this area). Due to the simplicity and rigidity, a single-link structure is recognized as the most efficient and reliable way to insert momentum into the system. Compared to the popular single-link approach, relatively less research has been done for multi-link tails although they generate higher momentum in theory, partially due to the complicated transmission design. For the current three multi-link tails, [9] is recognized as a rigid tail due to its gear coupling mechanism and [10, 11] are recognized as flexible tails due to their elastic backbone and springs. It turns out that the rigid one performs better in dynamics than the flexible ones. However, since they all use cables to transmit motion from the base to each link, even the rigid one suffers from the common cable driven issues like unidirectional driving and cable elasticity. Therefore, if we can find a multi-link structure that uses a rigid mechanism to transmit motion, the new tail might be able to possess both the single-link advantages (high frequency response, robust structure) and multi-link advantages (high momentum, dexterous mobility).

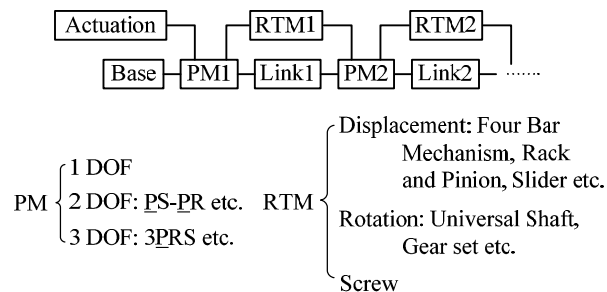


Figure 2. The rigid coupling hybrid mechanism concept

For this purpose, the difficulty is found in the transmission design, which requires transmitting motion for serially connected spatial mechanisms. To address this challenge, the RCHM is proposed, for which the core idea is to transmit motion from i^{th} link to $i + 1^{\text{th}}$ link instead of transmitting directly from the base to each link. This transmission is realized by the “rigid coupling” mechanism which couples the $i + 1^{\text{th}}$ link motion with i^{th} link motion. As for the basic mobility

requirements, like traditional hybrid mechanisms [14], the parallel mechanism part of the “hybrid mechanism” connects adjacent segments to achieve the required mobility. For instance, a three DOF spatial RCHM may be designed as a serially connected three DOF parallel mechanism with every adjacent parallel mechanisms coupled by three rigid mechanisms.

As shown in Fig. 2, the complete RCHM consists of five components: base, actuation, link, parallel mechanism (PM), and rigid transmission mechanism (RTM). The RTMs realize the “rigid coupling” tasks for adjacent PMs while the PMs realize the mobility tasks for the whole structure. Therefore, when the actuators drive the PM1, the RTM1 will take advantage of the PM1 motion to drive PM2. As long as PM2 moves, RTM2 transmits motion from PM2 to PM3, and so on and so forth.

There are many PM designs [15] based on different mobility requirements, while there are only limited choices for RTM designs. Fig. 2 lists several of the most useful designs including the four bar mechanism, the rack and pinion mechanism, slider mechanism for displacement transmission, and the universal shaft, the gear set for rotary transmission. For different applications, the PMs and RTMs could be chosen as the same or the different.

3 MECHANISM SYNTHESSES

Based on the proposed RCHM concept, this section presents the synthesis process of realizing the conceptual robotic tail design. By analyzing the maneuvering and stabilization task requirements, the new tail is desired to have a rigid structure and achieve uniform spatial bending (more specifically, the two DOF universal rotation), just like animal tails. Additionally, the new tail should be symmetric, reliable, and easy to manufacture.

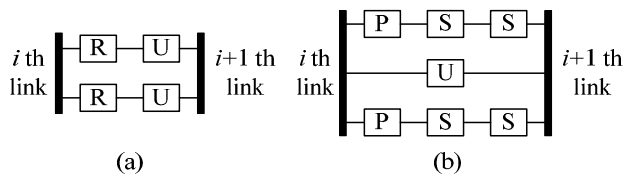


Figure 3. Two examples of 2DOF PM: (a) 2RU configuration, (b) 2PSS-U configuration.

3.1 Type Syntheses

Based on the RCHM concept, the first step is to synthesize the parallel mechanism with two DOF rotation (the universal rotation in specific). Depending on the number of kinematic chains, there are multiple candidates for this low mobility PM. For instance, if two identical kinematic chains are used to connect i^{th} link and $i + 1^{\text{th}}$ link, each chain should have three DOFs. For this case, 2RU or 2PU might be a solution. By applying the composite kinematic chains in [16, 20], more solutions may be obtained. However, considering the desired mobility is exactly the universal rotation, a natural solution might be to use the universal joint directly as the basic

kinematic chain and use another two chains to drive the universal joint. This yields the 2PSS-U structure. This structure has the benefits of large rotation angle and simpler kinematics. The two solutions are illustrated in Fig. 3.

The second step is to choose the appropriate rigid transmission mechanism to couple the motions between i^{th} link and $i + 1^{\text{th}}$ link. For this purpose, Fig. 2 lists several candidates for different transmission tasks. In our case, due to the tail length, transmitting displacement is easier than transmitting rotation. Therefore, the four bar mechanism, the rack and pinion mechanism, and the single slider mechanism are the most promising candidates. Fig. 4 illustrates the motion transmission of these mechanisms, where (b) and (d) follow the same motion direction and (a) and (c) reverse the direction.

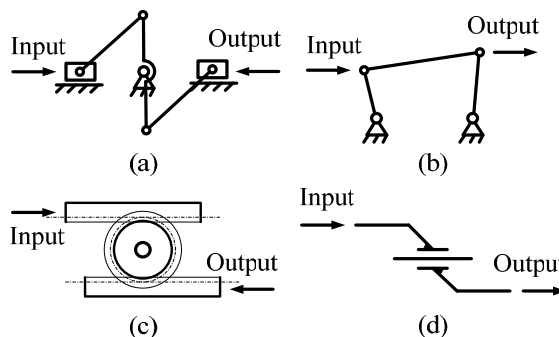


Figure 4. Potential RTMs for displacement transmission: (a) slider-crank mechanism for motion reversing, (b) double rocker mechanism for motion following, (c) rack and pinion mechanism for motion reversing, (d) single slider mechanism for motion following.

Different combinations of the PMs and RTMs generate different architectures of the final tail design. By considering both the mechanism simplicity and mechanical performance, the rigid tail mechanism is chosen as 2PSS-U being the PM and the slider mechanism being the RTM.

3.2 Mechanical Design

Based on the mechanism synthesized in Section 3.1, this section realizes the mechanical design by mainly considering the kinematic calculations and manufacturing cost.

The overall design of the new tail is shown in Fig. 5. The new tail is named Rigitail for presentation convenience. Rigitail consists of seven segments that connected serially by universal joints. The universal joint is driven by two perpendicular PSS chains which are denoted as chain A (in yellow) and chain B (in blue) respectively. Chain A and chain B along with the universal joint constitute the “driving” parallel mechanism (PM). To take advantage of the current segment motion for driving the next segment, an identical but head-to-head placed PM (sharing the same universal joint) is designed as the rigid coupling mechanism. This symmetric design brings in a unique kinematic advantage in that the input displacements for $i + 1^{\text{th}}$ segment

can be obtained by computing the inverse kinematics of the PM for exchanged negative rotation angles (see Section 4.2). Chain A and chain B are also designed to be identical so that the yaw and pitch rotations have the same property. Figure 6 illustrates the kinematic diagram of the adjacent segment connection mechanism.

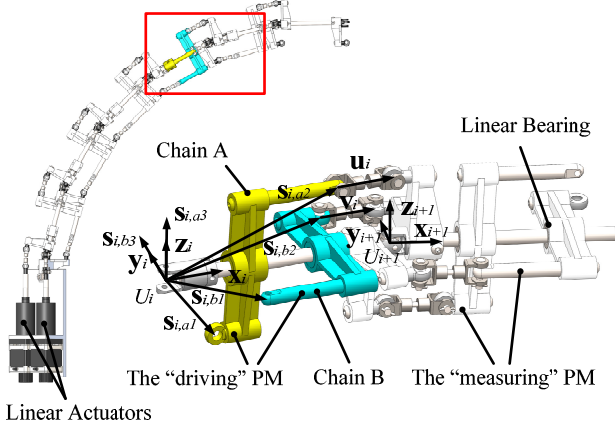


Figure 5. Mechanical design of the Rigitail. Two identical PMs are placed head-to-head to connect adjacent links, which facilitates the kinematic calculation significantly.

Another important design feature lies in the placement of the ball joint. As shown in Fig. 5, $s_{i,a3}$ has the same direction as z_i . This makes chain A become a planar mechanism with kinematics that are independent of chain B. However, chain B is still a spatial mechanism affected by chain A. This feature facilitates the kinematic computation of the PM and more importantly, allows changing the first ball joint to a revolute joint. By doing so, the slider no longer needs to be constrained by the shaft and thus reduces the manufacturing complexity. It is worth note that for the “measuring” PM, due to the symmetric design, chain B becomes the planar mechanism while chain A is the affected one.

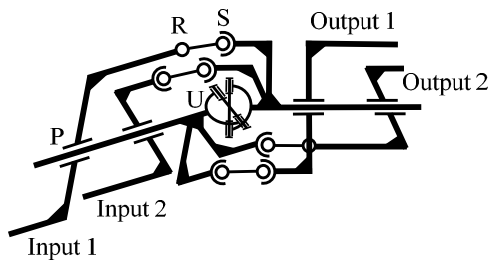


Figure 6. Kinematic diagram of the segment connection mechanism

4 KINEMATIC ANALYSIS

This section presents the kinematic model of the Rigitail. Due to the hybrid mechanism architecture and the uniform design of each segment, the kinematics are obtained recursively.

4.1 Closed Form Segment Wise Kinematics

In robotics, the kinematics problem usually consists of two sub problems: a) the forward kinematics that calculates the robot position and orientation by giving the actuator positions and b) the inverse kinematics that calculates the actuator positions based on the given robot pose. For traditional hybrid mechanism [14], due to the overall serial structure and the segment wise parallel structure, the kinematics is usually obtained recursively. That is, solving the segment wise kinematics first and then obtaining the overall kinematics by forward or inverse propagation. This technique is applied for this paper except that the Rigitail does not discriminate the forward or inverse kinematics.

Due to the symmetric design for chain A and chain B, the connection between adjacent segments essentially consists of two identical PMs placed head-to-head. One is for “driving” and the other is for “measuring” (their roles may be exchanged for different calculation purposes). Both have the same structure except in inverse proportional way. Due to this unique feature, the segment wise kinematic calculation needs both the forward and inverse kinematics of the PM. Mathematically, this requires two basic maps and their inverses: a) the map $\alpha(a_i)$ from a_i to rotation α_i (α_i only depends on a_i due to the decoupled design) and b) the map $\beta(\alpha_i, b_i)$ from a_i and b_i to β_i .

Based on the kinematic configuration defined in Fig. 5, the homogenous transformation of body fixed frame $\sum U_{i+1} = (U_{i+1}, x_{i+1}, y_{i+1}, z_{i+1})$ on link $i + 1$ respect to $\sum U_i$ is

$${}^i T_{i+1} = D_x(L)R_y(\alpha_i)R_z(\beta_i) \quad (1)$$

where R_z and R_y are the elementary rotational homogenous transformation for z axis and y axis respectively. $D_x(L)$ is the displacement homogenous transformation along x axis for the L quantity (link length). The necessary local vectors are given in Eq. 2 where R is the tail radius, a_i and b_i are the displacement variables for the prismatic joint A and B respectively.

$$\begin{aligned} {}^i s_{i,a2} &= [a_i \ 0 \ R \ 1]^T \\ {}^i s_{i,a3} &= [0 \ 0 \ R \ 1]^T \\ {}^i s_{i,b2} &= [b_i \ R \ 0 \ 1]^T \\ {}^i s_{i,b3} &= [0 \ R \ 0 \ 1]^T \end{aligned} \quad (2)$$

Therefore, the constraint equations are obtained as

$$\mathbf{u}_i^T \mathbf{u}_i = \mathbf{v}_i^T \mathbf{v}_i = e^2 + 1 \quad (3)$$

where e is the bar length between the two ball joints and

$${}^i \mathbf{u}_i = {}^i T_{i+1} {}^i s_{i,a3} - {}^i s_{i,a2} \quad (4)$$

$${}^i \mathbf{v}_i = {}^i T_{i+1} {}^i s_{i,b3} - {}^i s_{i,b2} \quad (5)$$

Solving Eq. 3 yields the two maps α and β

$$\alpha_i = \alpha(a_i) = \arccos \frac{2R^2 + (L - a_i)^2 - e^2}{2R\sqrt{R^2 + (L - a_i)^2}} - \operatorname{atan} \frac{L - a_i}{R} \quad (6)$$

may be defined to reflect the overall nonuniformity.

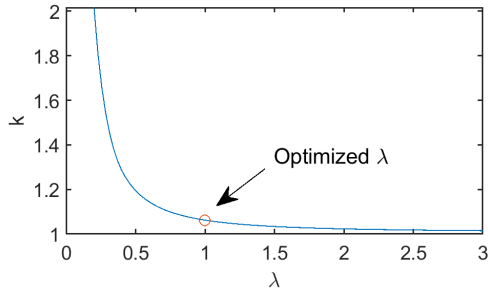


Figure 8. k is monotonic decreasing as λ increases

Simple computation (shown in Fig. 8) shows that k is monotonically decreasing as λ increases. However, k decreases slowly after $\lambda > 1$. From practice considerations, large λ shrinks the space for mounting two sliders. Therefore, the optimized λ is chosen as to be 1 as tradeoff. Figure 9 shows the nonuniformity distribution on region \mathcal{D} for $\lambda = 1$ and $\lambda = 0.3$. The maximum value 0.0173 appears at the region vertices (which is equivalent to $\max(\|\delta\mathbf{d}\|) = 0.33\text{mm}$ for the practical design).

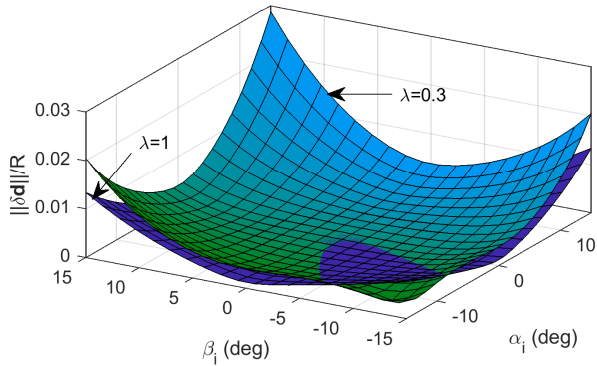


Figure 9. The $\|\delta\mathbf{d}\|/R$ distribution for optimized $\lambda = 1$ and non-optimized $\lambda = 0.3$.

5.2 Preliminary Dynamic Performance Evaluation

Since the Rigitail design is motivated by achieving maneuvering and stabilization tasks for legged robots, the dynamic performance is mainly measured by the momentum that the tail inserts into the system. Based on the optimized results, for small rotation angles, the segment bending is approximately uniform. Therefore, for the preliminary momentum calculations, all segments are assumed to have the same rotation angles and each segment could be simplified as an evenly distributed cylinder.

The moment of momentum [17] of the Rigitail is calculated by Eq. 17 where subscript “rt” stands for “rigid tail” (“pt” stands for “pendulum tail” for following equations). Since the first link does not contribute any momentum, the original is chosen as U_2 and the momentum starts from the second link. \mathbf{I}_i

is the i^{th} link moment of inertia respect to its center of mass (COM) and measured in the global frame.

$$\mathbf{h}_{rt} = \sum_{i=2}^7 (\mathbf{I}_i \boldsymbol{\omega}_i + m \mathbf{p}_{i,c} \times \mathbf{v}_{i,c}) \quad (17)$$

\mathbf{I}_i is computed by Eqs. 18-19 where m is the segment weight and \mathbf{R}_i is the orientation of i^{th} link.

$$\mathbf{I}_i = \mathbf{R}_i {}^i \mathbf{I}_i \mathbf{R}_i^T \quad (18)$$

$${}^i \mathbf{I}_i = \text{Diag}([0 \quad mL^2/12 \quad mL^2/12]) \quad (19)$$

$\boldsymbol{\omega}_i$, $\mathbf{p}_{i,c}$, and $\mathbf{v}_{i,c}$ are the corresponding segment angular velocity, COM position, and COM velocity respectively, which are calculated by Eqs. 20-25 where the initial condition is $\mathbf{p}_{2,u} = \mathbf{v}_{2,u} = \mathbf{0}_{3 \times 1}$.

$$\boldsymbol{\omega}_i = (i-1)\boldsymbol{\omega}_2 \quad (20)$$

$$\mathbf{p}_{i,u2u} = 2\mathbf{p}_{i,u2c} = \mathbf{R}_i [L \quad 0 \quad 0]^T \quad (21)$$

$$\mathbf{p}_{i,c} = \mathbf{p}_{i,u} + \mathbf{p}_{i,u2c} \quad (22)$$

$$\mathbf{v}_{i,c} = \mathbf{v}_{i,u} + \boldsymbol{\omega}_i \times \mathbf{p}_{i,u2c} \quad (23)$$

$$\mathbf{p}_{i,u} = \mathbf{p}_{i-1,u} + \mathbf{p}_{i,u2u} \quad (24)$$

$$\mathbf{v}_{i,u} = \mathbf{v}_{i-1,u} + \boldsymbol{\omega}_i \times \mathbf{p}_{i,u2u} \quad (25)$$

For a same length, same weight single-link pendulum tail, the moment of momentum is calculated as

$$\mathbf{h}_{pt} = \mathbf{I}_{pt} \boldsymbol{\omega}_2 + 6m \mathbf{p}_{pt,c} \times (\boldsymbol{\omega}_2 \times \mathbf{p}_{pt,c}) \quad (26)$$

where $\boldsymbol{\omega}_2$ indicates the same rotation as the second link of the Rigitail. The moment of inertia \mathbf{I}_{pt} and $\mathbf{p}_{pt,c}$ are given by

$$\mathbf{I}_{pt} = \mathbf{R}_2 \text{Diag}([0 \quad 18mL^2 \quad 18mL^2]) \mathbf{R}_2^T \quad (27)$$

$$\mathbf{p}_{pt,c} = \mathbf{R}_2 [3L \quad 0 \quad 0]^T \quad (28)$$

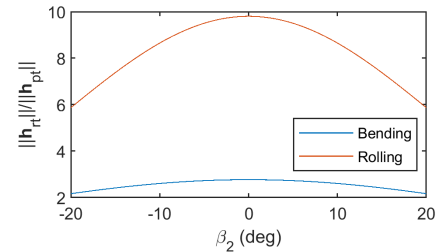


Figure 10. The momentum comparison between the Rigitail and the pendulum tail

To compare the momentum generated by the Rigitail and the pendulum tail, numerical computations of two typical cases are conducted: planar bending and rolling. As shown in Fig. 10, value $\|\mathbf{h}_{rt}\|/\|\mathbf{h}_{pt}\|$ is used to compare the momentum and different orientations β_2 are tested. It can be found that the Rigitail generates much larger momentum than the pendulum tail and the ratios maximize both at $\beta_2 = 0$. It is worth to note

that the rolling ratio is not defined at $\beta_2 = 0$ since both \mathbf{h}_{pt} and \mathbf{h}_{rt} are zero vectors at this point.

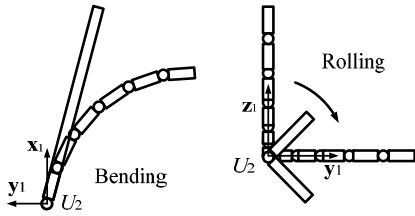


Figure 11. Two typical tail motions show that the multi-link structure generates more momentum than the single-link structure with the same input.

The advantages can be explained intuitively. As shown in Fig. 11, for the same rotation input, the Rigitail has a similar moment of inertia as the pendulum tail when bending. However, each segment in Rigitail possesses much larger velocity than the corresponding segment in the pendulum if the pendulum is regarded as a fixed connected multi-link structure. As for the rolling, although both structures have the same angular velocity, the Rigitail possesses much larger moment of inertia.

Note that in logic, this paper should end up with comparing the new tail with the flexible structure, cable driven tails to validate/falsify the claims/proposals presented in the introduction. However, this could only be done with the prototype being manufactured, which is the ongoing work of this research. Therefore, the purpose of this section is not to validate the claims in the introduction by comparing the new tail with the pendulum tail. Instead, this section is only intended to provide some preliminary information for future dynamic analysis.

6 CONCLUSION

By taking advantage of the traditional hybrid mechanism architecture and utilizing rigid mechanisms to couple the motions between i^{th} link and $i + 1^{\text{th}}$ link, this paper proposed a new multi-link rigid tail. The new tail realizes the rigid coupling hybrid mechanism concept with 2PSS-U being the parallel mechanism and the slider mechanism being the rigid transmission mechanism. By arranging the tail mechanism in such a manner, the new tail is able to achieve two DOF universal bending for each segment and is driven by only two linear actuators. Due to the rigid structure, the tail has promising potential in high stiffness, high speed application scenarios. The kinematic model was developed and an optimization process was conducted to minimize the bending nonuniformity. The simplified dynamic performance evaluation further validated the proposed dynamic potentials.

Future work will mainly focus on implementing a full scale prototype to evaluate the proposed highly dynamic performances. The validated prototype will then be mounted on a legged robot to further investigate its practical performances for maneuvering and stabilization tasks.

ACKNOWLEDGMENTS

This material is partially based upon the work supported by the National Science Foundation under Grants No. 1557312 and 1906727.

REFERENCES

- [1] Patel, A. and Boje, E., 2015, "On the conical motion of a two-degree-of-freedom tail inspired by the Cheetah," *IEEE Transactions on Robotics*, **31**(6), pp.1555-1560.
- [2] Saab, W., Rone, W.S. and Ben-Tzvi, P., 2018, "Robotic tails: a state-of-the-art review," *Robotica*, **36**(9), pp.1263-1277.
- [3] Liu, G.H., Lin, H.Y., Lin, H.Y., Chen, S.T. and Lin, P.C., 2014, "A bio-inspired hopping kangaroo robot with an active tail," *Journal of Bionic Engineering* **11**(4), pp.541-555.
- [4] De, A. and Koditschek, D.E., 2015, "Parallel composition of templates for tail-energized planar hopping," *ICRA 2015*, Seattle, USA, pp.4562-4569.
- [5] Liu, Y. and Ben-Tzvi, P., 2018, "Dynamic Modeling of a Quadruped with a Robotic Tail Using Virtual Work Principle," *IDETC/CIE 2018*, Quebec City, Canada, pp.V05BT07A021-V05BT07A021.
- [6] Libby, T., Moore, T.Y., Chang-Siu, E., Li, D., Cohen, D.J., Jusufi, A. and Full, R.J., 2012, "Tail-assisted pitch control in lizards, robots and dinosaurs," *Nature*, **481**(7380), p.181.
- [7] Briggs, R., Lee, J., Haberland, M. and Kim, S., 2012, "Tails in biomimetic design: Analysis, simulation, and experiment," *IROS 2012*, Vilamoura, Portugal, pp.1473-1480.
- [8] Rone, W. and Ben-Tzvi, P., 2016, "Dynamic Modeling and Simulation of a Yaw-Angle Quadruped Maneuvering With a Planar Robotic Tail," *Journal of Dynamic Systems, Measurement, and Control*, **138**(8), p.084502.
- [9] Saab, W., Rone, W.S., Kumar, A. and Ben-Tzvi, P., 2019, "Design and integration of a novel spatial articulated robotic tail," *IEEE/ASME Transactions on Mechatronics*, **24**(2), pp.434-446.
- [10] Rone, W.S., Saab, W. and Ben-Tzvi, P., 2018, "Design, Modeling, and Integration of a Flexible Universal Spatial Robotic Tail," *Journal of Mechanisms and Robotics*, **10**(4), p.041001.
- [11] Liu, Y. and Ben-Tzvi, P., 2019, "A Cable Length Invariant Robotic Tail Using a Circular Shape Universal Joint Mechanism," *Journal of Mechanisms and Robotics*, Accepted.
- [12] Rone, W.S., Liu, Y. and Ben-Tzvi, P., 2019, "Maneuvering and stabilization control of a bipedal robot with a universal-spatial robotic tail," *Bioinspiration & biomimetics*, **14**(1), p.016014.
- [13] Walker, I.D., 2013, "Continuous backbone 'continuum' robot manipulators," *Isrn robotics*, 2013.
- [14] Tanev, T.K., 2000, "Kinematics of a hybrid (parallel-serial) robot manipulator," *Mechanism and Machine Theory*, **35**(9), pp.1183-1196.
- [15] Merlet, J.P., 2006, *Parallel robots*. Springer.

- [16] Gao, F., Li, W., Zhao, X., Jin, Z. and Zhao, H., 2002, "New kinematic structures for 2-, 3-, 4-, and 5-DOF parallel manipulator designs," *Mechanism and machine theory*, **37**(11), pp.1395-1411.
- [17] Featherstone, R., 2014, *Rigid body dynamics algorithms*. Springer.
- [18] Saab, W., Rone, W. and Ben-Tzvi, P., 2018, "Discrete Modular Serpentine Robotic Tail: Design, Analysis and Experimentation", *Robotica*, **36**(7), pp. 994-1018.
- [19] Saab, W., Ben-Tzvi, P., 2016, "Design and Analysis of a Discrete Modular Robotic Tail for Improved Performance of Mobile Robots", *IDETC/CIE 2016*, Charlotte NC, USA, pp.V05AT07A061-V05AT07A061.
- [20] Kuo, C.H. and Dai, J.S., 2013, "Task-oriented structure synthesis of a class of parallel manipulators using motion constraint generator," *Mechanism and Machine Theory*, **70**, pp.394-406.